RSC Advances

ROYAL SOCIETY OF CHEMISTRY

www.rsc.org/advances

Journal Name

RSCPublishing

ARTICLE

Controlling the hydrothermal growth and the properties of ZnO nanorod arrays by pre-treating the seed layer

Cite this: DOI: 10.1039/xoxxooooox

Received ooth January 2012,
Accepted ooth January 2012

DOI: 10.1039/xoxxooooox

www.rsc.org/

Y. Yin,[a] Y. Sun,*[a] M. Yu,*[b] X. Liu,[a] B. Yang,[a] D. Liu,[c] S. Liu,[c] W. Cao [a,d] and M.N.R. Ashfold*[e]

Dense arrays of ultra-thin zinc oxide (ZnO) nanorods have been fabricated on *c*-oriented ZnO seed layers by hydrothermal growth, with particular emphasis on exploring the effects of annealing or plasma pre-treating the seed layer. Such pre-treatments influence the density, size and surface defects of particles within the nucleating seed layer, which impacts on the subsequent nanorod growth via sequential reaction with OH^- and Zn^{2+} species. Oxygen-rich defects at the seed layer surface are deduced to have particular impact – affecting both the *c*-axis growth rate and the photoluminescence properties of the as-grown nanorods.

1. Introduction

Zinc oxide (ZnO) nanorod (NR) arrays have attracted great attention over the past decade as a result of their many fascinating properties. Examples include their well-defined alignment, high surface to volume ratio, excellent light emission characteristics, negative electron affinity and good biocompatibility, which lead to applications in such diverse arenas as light-emitting devices,[1] photodetectors,[2] gas sensors,[3,4] biosensors,[5] generators,[6] field emission devices,[7,8] dye-sensitized solar cells,[9,10] *etc*. To optimize their performance, considerable effort has been expended in seeking to control and tune the morphologies, arrangement and properties of ZnO NR arrays. Traditional strategies have typically involved varying the synthesis parameters (*e.g.* growth temperature, precursor concentrations, *etc*)[11-13] and/or a diverse range of post-treatments.[14,15] Another widely used strategy is to grow on a pre-deposited seed layer; the density, size and arrangement of the seeds are found to influence the density, diameters and distribution of the resulting NR array.[16-24] A detailed understanding of the correlation between the seed layer characteristics and the growth rate, light emission properties, *etc*. of the resulting ZnO NRs remains elusive, however.

The present study employs *c*-oriented ZnO thin films deposited by magnetron sputtering as the seed layers for the subsequent fabrication of ZnO NR arrays by a hydrothermal method. Particular attention is devoted to exploring how different seed-layer treatments – Ar plasma treatment, annealing in an Ar atmosphere, and annealing in O_2 – affect the subsequent hydrothermal growth, and the photoluminescence (PL) properties, of the resulting ZnO NRs. Relative to NR arrays formed on an O_2-annealed seed layer, NRs grown on seed-layers treated with an Ar plasma are shown to exhibit enhanced *c*-axis (*i.e.* [001] direction) growth rates, and PL spectra with much higher UV/visible emission ratios. Mechanisms to account for these findings are proposed by considering how pre-treatment induced changes in surface defects affect the relative concentrations of Zn^{2+} and OH^- species adjacent to the polar surfaces during ZnO nanorod growth.

2. Experimental

ZnO thin films deposited on Si substrates using a radio-frequency (RF) magnetron sputtering method were employed as the seed layers. Si(100) substrates were first cleaned, sequentially, in acetone, ethanol and then water in an ultrasonic bath, then dried in a nitrogen gas flow. A ZnO thin film was then deposited onto the substrate maintained at T_{sub} = 400 °C by sputtering a ZnO ceramic target (99.99% purity) positioned 50 mm away using an applied RF power P = 150 W and an Ar/O_2 mixture (flow rates, F = 40 sccm and 10 sccm, respectively) at a pressure of 1 Pa for a time t = 1 h. After deposition, each as-grown sample was divided into four. One was retained unaltered, the other three were (i) treated with a pure Ar plasma (P = 50 W, at room temperature for t = 1 h), (ii) annealed in Ar and (iii) annealed in O_2. Both annealing treatments used F = 600 sccm, T_{sub} = 600 °C and t = 1 h.

ZnO NR arrays were synthesized by a hydrothermal method described previously.[15] Equimolar aqueous solutions (0.002 M, 50 mL) of zinc nitrate and hexamethylenetetramine (HMT), both 99% purity and supplied by Aladdin, China, were heated separately to 90 °C and then mixed in a 100 mL glass bottle. Substrates coated with the as-grown and the three treated seed films were immersed in the mixture and the bottle sealed and maintained at 90 °C for 3 hours. The resulting samples were then removed, rinsed by deionized water and dried by a freeze dryer (TFD550J, I1shin Lab, Korea) prior to characterization by scanning electron microscopy (SEM, FEI

Quanta 200F, 30 kV), transmission electron microscopy (TEM, TecnaiG2F30, 300 kV), atomic force microscopy (AFM, Asylum research, Cypher ES), X-ray diffraction analysis (XRD, PANalytical, X'Pert Pro, with Cu Kα radiation), and investigation of their PL emission using a spectrofluorometer (HORIBA, Fluoromax-4, exciting at 325 nm).

3. Results and discussion

3.1. The seed layers

The crystalline nature of the as-grown and the post-treated seed layers were characterized by XRD. As Fig. 1 shows, the ZnO (002) peak is dominant in all cases, indicating that all of these seed layers are *c*-axis aligned. Compared to the as-grown films (Fig. 1(a)), annealing in either Ar (Fig. 1(b)) or O_2 (Fig. 1(c)) leads to an obvious increase in the absolute intensity of the (002) diffraction peak – implying that annealing induces some improvement in crystallinity. Ar plasma treatment, in contrast, leads to a slight reduction in the (002) peak intensity (Fig. 1(d)), probably due to plasma etching. Overall, samples annealed in O_2 exhibit the highest (002) peak intensity and, as shown by AFM (Fig. 2), also show the largest average grain size (Fig. 2(c)).

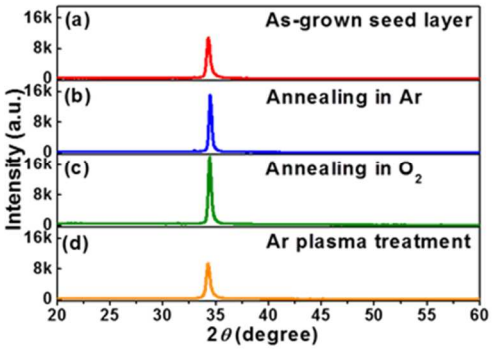

Fig. 1 XRD patterns of the as-grown and post-treated ZnO seed layers

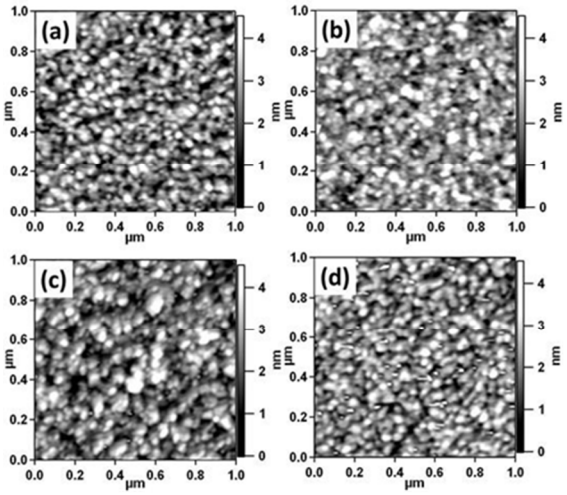

Fig. 2 AFM images of the four types of seed layer: (a) as-grown; (b) annealed in Ar (c) annealed in O_2, (d) Ar plasma treated.

3.2. The nanorods

ZnO NRs were synthesized on these four different seed layers simultaneously, in the same reactive solution containing equimolar zinc nitrate and HMT. ZnO NR growth under such conditions occurs exclusively on the nucleation sites supplied by the seed layers.[15] This synthetic strategy thus offers us a unique opportunity to explore, and to reveal, the impact of the seed layer on the growth, morphology, distribution, and performance of the resultant ZnO NRs. Fig. 3, which presents top view and (in the inset) cross-sectional SEM images of the NR arrays grown on each type of seed layer, reveals obvious differences in NR density and morphology. Average NR diameters and lengths derived from analysis of these four groups of samples are summarized in Table 1. TEM analysis reveals very similar morphology, and the characteristic 0.26 nm (002) lattice spacing of wurtzite ZnO, for all four samples – as illustrated by the example shown in Fig. 4.

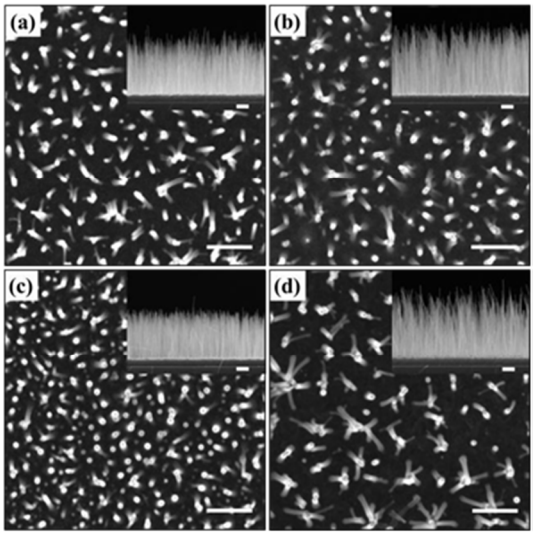

Fig. 3 Top view and (inset) cross-sectional SEM images of ZnO nanorods grown on (a) the as-grown seed layer, and on seed layers treated by (b) annealing in Ar, (c) annealing in O_2, and (d) Ar plasma treatment. The scale bar in each plan view SEM image indicates 200 nm.

Table 1 Average density, diameters and lengths of the ZnO NRs formed on the as-grown and pre-treated seed layers

Seed layer	Average density (μm^{-2})	Average diameter (nm)	Average length (μm)
As-grown	136±13	23±3	~1.0
Annealed in Ar	136±10	25±3	~1.1
Annealed in O_2	180±16	27±3	~0.8
Ar plasma treatment	113±9	25±3	~1.2

Given that all four samples were grown from a common reactive solution, any differences in NR morphology must be attributable to differences in the nucleating seed layers. The densest NR arrays are formed on seed layers annealed in O_2 (Fig. 3(c)). These NRs also show the largest average diameter, consistent with the evident grain growth during annealing in O_2 shown in Figs. 1(c) and 2(c). Such a finding accords with previous reports that the density and size of the nuclei comprising the seed layer have a marked influence on the array density and the NR diameters.[17,19,21] However, Table 1 also shows that growth on the seed layer annealed in Ar results in a similar density of NRs that, on average, are slightly longer and thicker than when using an unprocessed seed layer – hinting that the array density is not necessarily correlated with the NR heights and diameters.

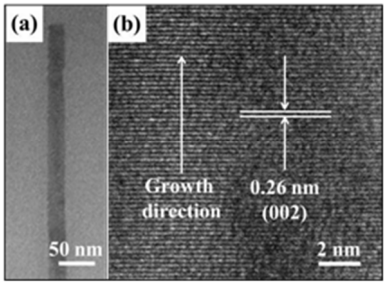

Fig. 4 (a) TEM and (b) high-resolution TEM image of a ZnO nanorod grown on the as-deposited seed layer.

Table 1 also highlights that the NR lengths (*i.e.* the NR growth rates, given that all grow from a common reactive solution for the same length of time) is seed layer dependent. The average length of NRs grown on the seed-layers annealed in O_2 is ~0.8 μm (*i.e.* notably shorter than those on the as-grown seed layers (~1.0 μm)), while NRs grown on the seed layers that had been annealed in Ar or Ar plasma treated are, on average, longer (~1.1 μm and ~1.2 μm, respectively). The influence of the seed layer on NR length has been reported previously,[25] though discussion of the mechanistic causes remains limited.

3.3. Photoluminescence properties

Fig. 5 shows PL spectra from the four different seed layers. Each displays a sharp near-UV peak from near-band-edge emission centered at ~387 nm along with a broad, orange-red emission that maximizes ~630 nm. All treatments enhance the UV peak emission intensity (I_{UV}) relative to that from the as-grown seed layer, most noticeably in the case of Ar plasma treatment. Arguably more revealing, we see that the intensity of the orange-red emission intensity (I_{vis}) is also affected by the various seed-layer treatments: I_{vis} is substantially increased by annealing in O_2 but reduced by Ar plasma treatment. These findings are consistent with earlier suggestions that the orange-red emission originates from oxygen-rich related defects, *e.g.* oxygen interstitials.[26,27] The I_{UV}/I_{vis} ratio of the seed layers annealed in O_2 (~0.6) is only about half that from the as-grown seed layers (~1.2), consistent with oxygen diffusion into the seed-layer during O_2 plasma treatment and the formation of additional oxygen-rich related defects. Seed layers subjected to Ar plasma treatment, in contrast, show much larger I_{UV}/I_{vis} ratios (~10), which we explain by assuming that such plasma treatment reduces the density of such defects.

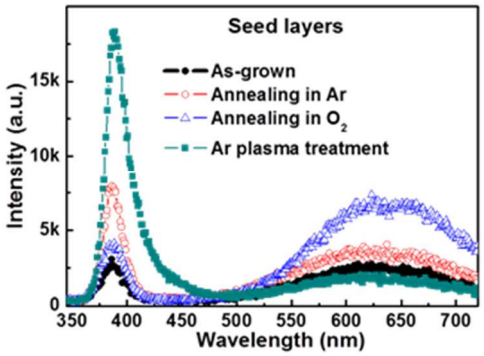

Fig. 5 PL spectra of the as-grown and treated ZnO seed layers.

PL spectra of the ZnO NRs grown on the four types of seed layers are shown in Fig. 6. Each of these spectra shows an obvious blue-shift relative to the PL spectrum of the corresponding seed layer; the peak of the near-UV emission decreases by ~5 nm (to ~382 nm), while the maximum of the visible emission shifts by ~50 nm (now maximising at ~580 nm). These differences are largely attributable to the different synthesis methods used for the seed layer (sputtering) and the NRs (hydrothermal growth). At a more detailed level, we note differences between the various PL spectra. The peak emission from each sample is at least 10-times that from its seed layer. Thus it is safe to conclude that PL from the seed layer itself is making, at most, a minor contribution to the spectra shown in Fig. 6 but this then begs the question: what is the trigger for the obvious differences in the PL spectra from these four NR samples?

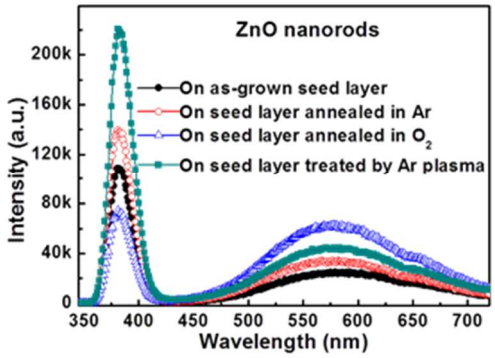

Fig. 6. PL spectra of ZnO nanorods formed on as-grown and treated ZnO seed layers.

One possibility might be differences in surface to volume ratio: greater NR surface to volume ratios have previously been reported to result in a lower I_{UV}/I_{vis} ratio.[28] Such an explanation obviously conflicts with the present data, however. The PL spectra from the NRs grown on the seed layer annealed in O_2 display the smallest I_{UV}/I_{vis} ratio, but these NRs are also thicker and shorter (*i.e.* have a smaller surface to volume ratio) than the NRs on the as-grown seed layer. The NRs with largest surface to volume ratio are those grown on the Ar plasma treated seed layer, yet these also exhibit the largest I_{UV}/I_{vis} ratio. Given these observations, and the fact that the NR samples were all grown from the same reactive solution, we conclude that the differences in the PL spectra reflect differences in the defects contained within the various NR samples, and that these latter differences must trace back to differences in the nucleating seed layers – indicating that O-rich related defects, (*e.g.* oxygen interstitials) at or near the surface of the seed-layer carry through into the subsequent NR formation and growth.

3.4. Mechanistic considerations

The wurtzite structure of ZnO comprises alternating layers of tetrahedrally coordinated O^{2-} and Zn^{2+} ions arranged normal to the c-axis. The uppermost (001) polar surface can be either positively (Zn-terminated) or negatively charged (O-terminated), and this choice can be expected to influence the Zn^{2+}/OH^- ratio in the solution boundary layer, and thus the local surface reactivity, electrostatic affinity, *etc*.[29] The NRs in the present work were grown from dilute equimolar solutions of zinc nitrate and HMT (0.001 M). The kinetics of hydrothermal growth under this condition has been discussed previously.[30] The pH value of the solution (~5.4) changes little during the growth process, so most of the zinc species in solution are in

the form of Zn^{2+} ions. ZnO NR growth under this condition then follows the reaction:

$$Zn^{2+} + 2OH^- \leftrightarrow ZnO + H_2O \quad (1)$$

The pH of the reactive solution used for NR growth implies an OH^- concentration (~$10^{-8.6}$ M) that is several orders of magnitude lower than that of Zn^{2+} (~10^{-3} M). Thus the rate of NR growth according to reaction scheme (1) will be controlled by the availability of OH^- ions. Further, it is rational to suggest that the OH^- concentration will be (relatively) lower in the boundary layer adjacent to a polar surface containing more O-rich related defects. Such expectations accord with the present observations: NRs grown on seed layers annealed in O_2 have the shortest lengths (*i.e.* lowest c-axis growth rate) and the smallest I_{UV}/I_{vis} ratio, while the seed layers treated with an Ar plasma (which we deduce to have the lowest density of O-rich related defects) support the longest NRs with the largest I_{UV}/I_{vis} ratio. Thus the present data implies that appropriate treatment of the nucleating seed layer offers some control over the optical and electrical properties of hydrothermally grown ZnO NRs.

Conclusions

Detailed studies of ZnO NRs grown by hydrothermal methods from a common reactive solution illustrate the extent to which the NR morphologies, and their PL properties, can be influenced by pre-treating the nucleating seed layer with, for example, an Ar plasma or by annealing in Ar (or O_2). Different pre-treatments result in differences in surface termination and in the nature and densities of surface defects, which are reflected both in the rate of hydrothermal growth of ZnO NRs nucleated from such surfaces, and the PL properties of the NRs. Most strikingly, the PL analysis within the present work reveals a propensity for O-rich defects (which are enhanced (reduced) by O_2 annealing (Ar-plasma-treating) the seed-layer) to:

(i) map through into the eventual NRs, and

(ii) reduce the NR growth rate – an effect we attribute to a relative reduction in the OH^- ion concentration in the boundary layer adjacent to the growing polar surface.

The present findings provide new, detailed and potentially valuable insights into ways of controlling the hydrothermal growth of ZnO NRs, and of optimizing the material properties for application in practical devices.

Acknowledgements

Financial support for this work was provided by the National Natural Science Foundation of China (grant no.11104046), the National Basic Research Program of China (973 Program) (grant no.2013CB632900) and by the Fundamental Research Funds for the Central University (grant nos. HIT.BRETIII.201216, HIT.BRETIII.201225 and HIT.BRETIV.201313). M.Y. thanks the Young Thousand Plan for financial support.

Notes and references

[a] Condensed Matter Science and Technology Institute, School of Science, Harbin Institute of Technology, Harbin 150080, China
E-mail: sunye@hit.edu.cn
[b] State Key Laboratory of Urban Water Resource and Environment, School of Chemical Engineering and Technology, Harbin Institute of Technology, Harbin 150001, China
E-mail: miaoyu_che@hit.edu.cn
[c] Key Laboratory of Microsystems and Microstructures Manufacturing, Harbin Institute of Technology, Harbin 150080, China
[d] Materials Research Institute, The Pennsylvania State University, University Park, Pennsylvania16802, U.S.A.
[e] School of Chemistry, University of Bristol, Bristol BS8 1TS, U.K.
E-mail: mike.ashfold@bristol.ac.uk

1 Q. Yang, Y. Liu, C. F. Pan, J. Chen, X. N. Wen and Z. L. Wang, *Nano Lett.*, 2013, **13**, 607.
2 L. Peng, L. F. Hu and X. S. Fang, *Adv. Mater.*, 2013, **25**, 5321.
3 C. M. Chang, M. H. Hon and I. C. Leu, RSC Adv., 2012, **2**, 2469.
4 S. Q. Tian, F. Yang, D. W. Zeng, C. S. Xie, *J. Phys. Chem. C*, 2012, **116**, 10586.
5 R. Ahmad, N. Tripathy, J. H. Kim and Y. B. Hahna, *Sens. Actuators B*, 2012,. **174**, 195.
6 D. Jang, J. Yoon, D. Kim, Y. S. Moon, K. H. Kim and J. S. Ha, *J. Mater. Chem. C*, 2013, **1**, 7191.
7 J. O. Hwang, D. H. Lee, J. Y. Kim, T. H. Han, B. H. Kim, M. Park, K. No and S. O. Kim, *J. Mater. Chem.*, 2011, **21**, 3432.
8 C. X. Zhao, Y. F. Li, Y. C. Chen, J. Q. Wu, B. Wang, F. T. Yi, S. Z. Deng, N. S. Xu and J. Chen, *Nanotechnology*, 2013, **24**, 275703.
9 S. Zhu, L. M. Shan, X. N. Chen, L. He, J. J. Chen, M. Jiang, X. L. Xie and Z. W. Zhou, *RSC Adv.*, 2013, **3**, 2910.
10 S. H. Ko, D. Lee, H. W. Kang, K. H. Nam, J. Y .Yeo, S. J. Hong, C. P. Grigoropoulos and H. J. Sung, *Nano Lett.*, 2011, *11*, 666.
11 F. Xian, W. F. Bai, L. H. Xu, X. X. Wang and X. Y. Li, *Mater. Lett.*, 2013, **108**, 46.
12 S. C. Liu and J. J. Wu, *J. Mater. Chem.*, 2002, **12**, 3125.
13 S. Cho, S. H. Jung and K. H. Lee, *J. Phys. Chem. C.*, 2008, **112**, 12769.
14 P. Sundara Venkatesh, S. Balakumar and K. Jeganathan, *RSC Adv.*, 2014, 4, 5030.
15 Y. Sun, N. G. Ndifor-Angwafor, D. J. Riley and M. N. R. Ashfold, *Chem. Phys. Lett.*, 2006, **431**, 352.
16 J. N. Ding, Y. B. Liu, C. B. Tan and N. Y. Yuan, *Nanoscale Res. Lett.*, 2012, **7**, 368.
17 R. Erdélyi, T. Nagata, D. J. Rogers, F. H. Teherani, Z. E. Horváth, Z. Lábadi, Z. Baji, Y. Wakayama and J. Volk, *Cryst. Growth Des.*, 2011, **11**, 2515.
18 L. W. Ji, S. M. Peng, J. S. Wu, W. S. Shih, C. Z. Wu and I. T. J. Tang, *Phys. Chem. Solids*, 2009, **70**, 1359.
19 H. Ghayour, H. R. Rezaie, S. Mirdamadi and A. A. Nourbakhsh, *Vacuum*, 2011, **86**, 101.
20 D. B. Zhang, S. J. Wang, K. Cheng, S. X. Dai, B. B. Hu, X. Han, Shi Q and Du Z L, *ACS Appl. Mater. Interfaces*, 2012, **4**, 2969.
21 C. Li, G. J. Fang, J. Li, L. Ai, B. Z. Dong and X. Z. Zhao, *J. Phys. Chem. C*, 2008, **112**, 990.
22 Y. S. Bae, D. C. Kim, C. H. Ahn, J. H. Kim and H. K. Cho, *Surf. Interface Anal.*, 2010, **42**, 978.
23 S. Guillemin, L. Rapenne, H. Roussel, E. Sarigiannidou, G. Brémond and V. Consonni, *J. Phys. Chem. C*, 2013, **117**, 20738.
24 S. Y. Liu, T. Chen, J. Wan, G. P. Ru, B. Z. Li and X. P. Qu, *Appl. Phys. A*, 2009, **94**, 775.
25 D. Y. Kim, J. Y. Kim, H. Chang, M. S. Kim, J. Y. Leem, J. Ballato and S. O. Kim, *Nanotechnology*, 2012, **23**, 485606.
26 T. Ghosh, M. Dutta and D. Basak, *Mater. Res. Bull.*, 2011, **46**, 1039.
27 T. Li, T. S. Herng, H. K. Liang, N. N. Bao, T. P. Chen, J. I .Wong, J. M. Xue and J. Ding, *J. Phys. D: Appl. Phys.*, 2012, **45**, 185102.

28 I. Shalish, H. Temkin and V. Narayanamurti, *Phys. Rev. B*, 2004, **69**, 245401.
29 M. N. R. Ashfold, R. P. Doherty, N. G. Ndifor-Angwafor, D. Riley and Y. Sun, *Thin Solid Films,* 2007, **515**, 8679.
30 Y. Sun, D. J. Riley and M. N. R. Ashfold, *J. Phys. Chem. B*, 2006, **110**, 15186.